Asian Journal of Electrical Sciences
ISSN: 2249-6297 (P); 2583-7923 (E)
Vol.13 No.1, 2024, pp.17-25

www.crijournals.org
DOI: https://doi.org/10.70112/ajes-2024.13.1.4230

Performance Analysis of a Solar-Powered Rotary Drum Composter for Optimized Food Waste Management

Ma. Angelica B. Danga[1], John Kevin C. Lim[2], Jude Milbert C. Jingco[3], Justine Roi P. Manalo[4], Joshua G. Marquez[5], Alma L. Tangcuangco[6], Genesis M. Tiria[7] and Jezeth Vince B. Macaspac[8]
[1,2,3,4,5,6&7]Department of Electrical Engineering, [8]Department of Mechanical Engineering,
Don Honorio Ventura State University, Philippines
E-mail: 2020100950@dhvsu.edu.ph
(Received 21 January 2024; Revised 25 February 2024; Accepted 8 March 2024; Available online 22 March 2024)

***Abstract* - The annual value of food waste generated worldwide has already reached a staggering $1 trillion. This amounts to 1.3-1.4 billion tons, or one-third of the food produced for human consumption, that goes to waste each year. The Food Center at Don Honorio Ventura State University faces a similar issue, with a weekly production of 21.5 kg of food waste. To address this increasingly concerning issue, a solar-powered rotary drum composter driven by a DC motor was developed. This composter is designed to accommodate up to 20 kg of food waste. Analysis of the composter's motor performance reveals significant relationships between voltage, current, speed, torque, efficiency, and load. The voltage exhibits an inversely proportional relationship with the load, steadily decreasing from 24.8 V to 23.3 V as the load increases, while the current shows a directly proportional relationship, consistently rising from 4.1 A to 9.84 A with the increased load. Further examination of torque and speed in relation to load indicates a directly proportional and inversely proportional relationship, respectively. Torque increases from 6.68 Nm to 27.23 Nm with increasing load, while speed decreases from 72.74 rpm to 55.16 rpm. As for efficiency, it was found that the composter operates most efficiently when the drum is loaded with 12 kg, beyond which efficiency gradually declines with increasing load up to 20 kg. This decline signifies the diminishing returns associated with higher loads, highlighting the importance of load optimization for sustained efficiency in composter operation.**
Keywords: **Natural Surfactants, Enhanced Oil Recovery, Saponin, Citrus Sinensis, Carica Papaya**

I. INTRODUCTION

The annual value of food waste generated worldwide has already reached a staggering $1 trillion [1]. This amounts to 1.3-1.4 billion tons, or one-third of the food produced for human consumption, that goes to waste each year [2]. Of this food wasted each year, around 13 percent is lost between the harvest and retail stages, while the rest is wasted at the consumer level.

An estimated 17 percent of global food production becomes waste in households, food services, and retail combined [2], [3]. These numbers are at risk of further escalation due to the growth in the global economy and population [4], with projections indicating a potential increase to as much as 2.6 billion tons by 2025 [5].

If food waste were a nation, it would rank as the third-largest contributor to greenhouse gas emissions, trailing only China and the United States [6]. Of the total annual food waste production, a significant portion, amounting to 275 million tons, is accounted for in South and Southeast Asia, where the Philippines is part of [3].

This worldwide concern regarding food waste is similarly evident in the country, which, if not addressed, could result in compounding challenges. In 2016, the typical Filipino family generated 66.8 g of plate waste each day, which is 5.0 g more than in 2015. It was disclosed that among typical plate waste, cereals and cereal products constituted 48.0 g, while fish, meat, and poultry accounted for 8.9 g. Additionally, 7.2 g consisted of vegetables, with the remaining 2.7 g representing various other food categories [7], [8].

TABLE I UNIVERSITY FOOD CENTER'S GENERATED WASTE FOR 5 DAYS IN KG

Type of Waste	Monday	Tuesday	Wednesday	Thursday	Friday	Total
Paper Cups	1.5	2	1.8	2.2	1.3	8.8
PET Bottles	4	3.75	2.5	2	2.8	15.05
Plastic Wrappers	1	0.6	0.75	0.5	0.5	3.35
Food Waste	5	5	4.25	3.75	3.5	21.5
Residual	14.5	8.8	9	13.4	11	56.7

The Food Center at Don Honorio Ventura State University faces a similar issue, as indicated in Table I. The University Food Center generates various types of waste, including 8.8 kg of paper cups, 15.05 kg of PET bottles, 3.35 kg of plastic

wrappers, 21.5 kg of food waste, and 56.7 kg of residual waste over five days. Although the quantity of residual waste surpasses that of food waste, the importance of prioritizing food waste processing is underscored by its composition. Food waste predominantly consists of solid materials, such as leftover rice and chicken meat, which are more challenging to manage and have a potentially higher environmental impact than liquid substances found in residual waste, such as water and sauces. Solid food waste in landfills can lead to the generation of methane, a potent greenhouse gas that contributes to climate change [9]. The anaerobic conditions in landfills facilitate methane production during the decomposition of organic solid waste [9].

Meanwhile, liquid residual waste generally decomposes aerobically, producing less methane compared to the anaerobic decomposition of solid waste. Moreover, leachate - the liquid that drains from landfills - can be more concentrated and environmentally harmful when derived from the decomposition of solid food waste, containing higher levels of organic pollutants than those from residual waste [10], [11].

To address this increasingly concerning issue, a solar-powered rotary drum composter driven by a DC motor, tailored to process the University Food Center's food waste, was developed. This study aims to design and construct a solar-powered rotary drum composter for processing food waste generated by the University Food Center, with a focus on the electrical aspect of the design to ensure autonomous sustainability. Specifically, this study aims to determine the following motor parameters when the drum is loaded with 0 kg, 4 kg, 8 kg, 12 kg, 16 kg, and 20 kg of compost: (1) the voltage and current across the motor terminals, (2) the speed and continuous output torque of the motor, and (3) the efficiency of the motor at different loads and the relationship between the speed of the drum and composting time.

This solar-powered rotary drum composter is designed to process various food wastes, such as vegetable scraps (e.g., carrot peels, potato skins, lettuce leaves, broccoli stems, onion skins, celery stalks), fruit waste (e.g., apple cores, banana peels, citrus rinds, melon rinds, grape stems), coffee grounds, tea bags, bread, grains, nut shells, stale bread, leftover rice, and eggshells. The composter runs for at least 10 minutes per day, which is a promising technique for decentralized composting [12], introducing agitation, aeration, and mixing of the compost. This process results in a consistent and uniform end product [12]-[14]. The rotation of the drum facilitates the inflow of ambient air, fostering an oxygen-rich environment within the drum, which is crucial for the bacteria responsible for composting. This drastically reduces composting time to 2-3 weeks [12], compared to traditional methods. Simultaneously, the process results in the emission of greenhouse gases, including CO2 and methane, generated by microbial activity as part of the outflow.

Numerous research studies have explored the development of composting apparatus with the objective of converting food waste into compost. For example, a study in [15] involved a rotary drum composter made of galvanized steel, approximately 170 L in capacity, with two chambers, developed and utilized for composting at home as a way to manage organic waste. The research focused on the design and implementation of this home composter. In [16], another rotary drum was designed and developed to manage household waste. However, this rotary drum is autonomous, solar-powered, and equipped with a remote management system to enable real-time monitoring and control of the composting process. Lastly, in [17], a similar rotary drum composter was also developed with a tracking system but without a battery.

The development of a solar-powered composter tailored for the University Food Center's food waste offers a dual advantage. Firstly, it contributes to a tangible reduction in the waste output of the food center. Secondly, it aligns with sustainability and renewable energy initiatives on campus, making it a potential cornerstone in the university's waste management system. Furthermore, this innovation sets an inspiring example for other institutions seeking to minimize their environmental footprint. Lastly, the utilization of the machine produces a final product that can be used as organic fertilizer [15]-[17] at a nearby local farm, improving soil properties and making it a valuable product for agricultural applications [18].

II. METHODOLOGY

To accomplish a successful research project leading to the development of a solar-powered composter, data on the UFC's five-day generated waste was collected and categorized by waste type. From this data, the volume of food waste input into the composter was considered for specifying the composter. The materials and electrical components needed to develop the composter were then identified.

Additionally, according to [15], the most optimal mixture of organic waste for composting in a rotating drum is a food waste-to-bulking agent mass ratio of 1:0.5. This ratio achieves better results in terms of waste volume reduction, which is seen as a positive feature as more waste can be treated. Moreover, if available, it is recommended to add animal manure, at least 10% of the volume of the food waste, to enhance the degradation of organic matter. In case the compost emits a strong foul odor, the addition of charcoal can help reduce it.

A. Solar-Powered Rotary Drum Components

As seen in Fig. 1, the solar-powered rotary drum comprises several key components that facilitate its operation. These components are categorized into two main groups: the rotating mechanism and the electrical components. The rotating mechanism includes the drum, DC motor, and

sprocket, all working in tandem to drive the motion of the drum. On the other hand, the electrical components consist of a battery, solar panels, a control box, and necessary wiring with overcurrent protection devices. Together, these components form a cohesive system, harnessing solar energy to power the rotary drum.

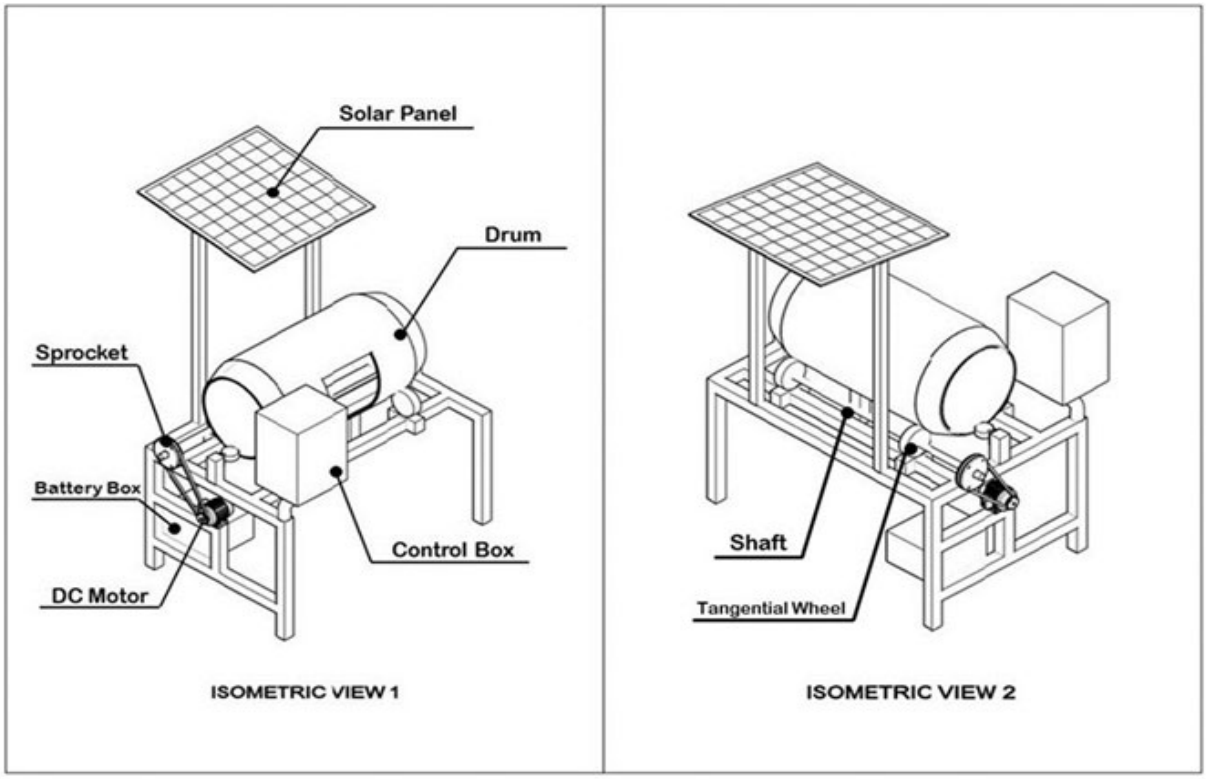

Fig. 1 Frame Design of Solar-Powered Rotary Composter

B. Rotating Mechanism

1. Drum

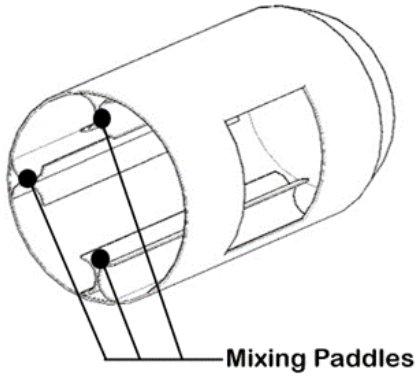

Fig. 2 Drum Design

Formula (1) is used to determine the minimum volume of the drum, considering the weight and density of the input food waste, which is a maximum of 20 kg and 290 kg/m³ [3], respectively. Therefore, a 170 L PVC drum was used. Moreover, a 50% [16] allowance is made to the drum's volume for the opening of the drum during loading.

$$V_{drum} = \frac{Drum_{full\ capacity\ (kg)}}{\rho_{food\ waste}} x\ 150\% \quad (1)$$

To ensure thorough mixing of the compost, three sets of mixing paddles crafted from PVC tubes, 29 inches in length and 5 inches in width, were riveted onto the drum's walls, positioned approximately 90 degrees apart from each other.

2. DC Motor: The motor that will drive the system was determined by Formula (2), which depends on the predetermined speed of the rotary drum, the torque requirement to rotate the drum at full load, and a 1.5 safety factor for the DC motor [19]. Hence, a 250-W motor with nameplate values of 24 VDC, 330 rpm, and 13 A full-load current was used.

$$P_M = \frac{2\pi NT}{60} x\ 1.5 \quad (2)$$

3. Sprocket: To meet the necessary speed and torque requirements to drive the drum, a reduction gear will be used to connect the motor and the shaft of the axle that will rotate the drum. The reduction ratio depends on the ratio of the rated speed of the motor under normal conditions to the rotational speed of the drum (3). The motor has a rated speed of 330 rpm and must be reduced to at least 10 rpm, as recommended in [15, 16, 17]. Hence, a gear reduction ratio of at least 33:1 is required.

$$G.R. = \frac{N_1}{N_2} = \frac{T_2}{T_1} \quad (3)$$

C. Electrical Components

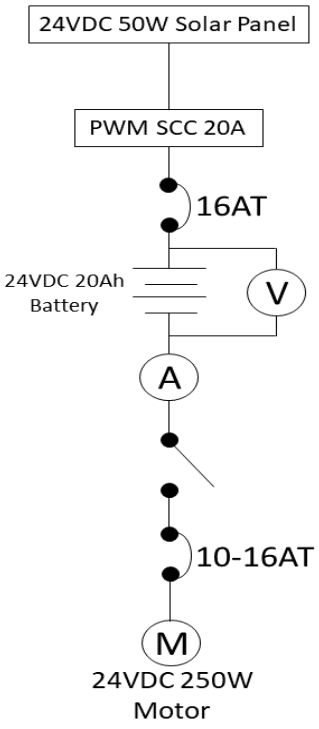

Fig. 3 Single-Line Diagram

The electrical system that supplies power to the 24 V DC motor is composed of two 12 V 25 W solar panels connected in series, two 12 V 20 Ah lead-acid batteries connected in series to ensure that the system can autonomously run for at least four days, and a solar charge controller that regulates the current for charging the batteries.

1. Battery Bank: As shown in Formula (4), when selecting the power bank, four key factors were considered: the chosen system voltage, total demand energy (T.D.E.), days of autonomy (D.o.A.), and depth of discharge (D.o.D.). A 24 V system was used due to the motor's nominal voltage requirement. T.D.E. was calculated based on the motor's power rating, daily operating hours, and the cumulative percent loss across system components. Additionally, a four-day autonomy period and a 50% depth of discharge were established, given the use of a lead-acid battery [20].

$$Ah = \frac{(T.D.E.)(D.o.A.)}{(D.o.D.)(24V)} \quad (4)$$

$$T.D.E. = (P_m)\left(\frac{Operating\ Hours}{Day}\right)(1 + \sum \%loss) \quad (5)$$

2. Solar Panel Rating: For a 24 V system, the minimum solar panel rating required to charge the battery can be calculated using Formula (6). This rating is influenced by factors such as the capacity of the battery bank (set at 20 Ah), the depth of discharge (D.o.D.) of the battery, and the peak sun hours [20], which in the Philippines range from 4.5 to 5 hours [21].

$$Solar\ Panel\ Rating = \frac{(24V)(Ah)(D.o.D.)}{Peak\ sun\ hours} \quad (6)$$

3. Solar Charge Controller: The minimum rating for the solar charge controller was determined by multiplying a 125% safety factor by the short-circuit current rating I_{SC} of the PV module and the number of PV modules in parallel connection [22, 23]. Since the I_{SC} rating of a 12 V 25 W module was 1.49 A, and there was only one string of PV modules connected in series, the minimum rating of the solar charge controller should be 1.86 A. However, since no solar charge controller with this specific rating was available, the next higher available rating, which was 20 A, was chosen for use.

$$SCC\ rating = (1.25)(I_{sc})(\#\ of\ parallel\ PV) \quad (7)$$

4. Control Panel: The control system for the motor is equipped with four buttons, namely PB1, PB2, PB3, and PB4. PB1, designated as the emergency stop, halts the machine in the event of an emergency or unsafe conditions. This button initiates a rapid shutdown process, cutting off power to all essential components to ensure a swift and effective response to potential hazards, prioritizing the safety of both the machine and its operators. Distinguished by a mushroom-shaped head and a prominent red color, PB1 is easily accessible for quick identification. In contrast, PB2 serves as the stop button, providing general control within the regular interface and facilitating routine halting of the machinery for planned activities or maintenance.

PB3 serves as the start button for the machine, activating its operation. Pressing PB3 energizes the K3 relay, causing the closure of the K3 contactor, which is connected to the motor, and initiating current flow. This current triggers a multifunction timer relay, TR, which has been integrated to restrict the machine's operation to the necessary duration for compost mixing. The relay is set with an on-delay feature and linked to a normally closed contactor coil. The machine continues to operate until the contactor coil opens at the predetermined time set for the relay. This methodical sequence ensures controlled and timed operation of the machine. Meanwhile, PB4 functions as the jog button, allowing operators to manually and momentarily move the drum. This feature enables precise adjustments when the drum's position makes it inconvenient for operators to load food waste.

The machine also features four LED indicators: H1, H2, H3, and H4. H1 (White LED) signifies the availability of power for the machine. H2 (Yellow LED) signals a system fault, indicating that either the SLS is inactive or CB3 is open or tripped. H3 (Green LED) illuminates when the machine is powered on and operational, while H4 (Red LED) indicates available power but signifies that the machine is currently not in operation. Additionally, a digital meter for voltage and current has been incorporated into the control panel to monitor the motor's voltage and current levels.

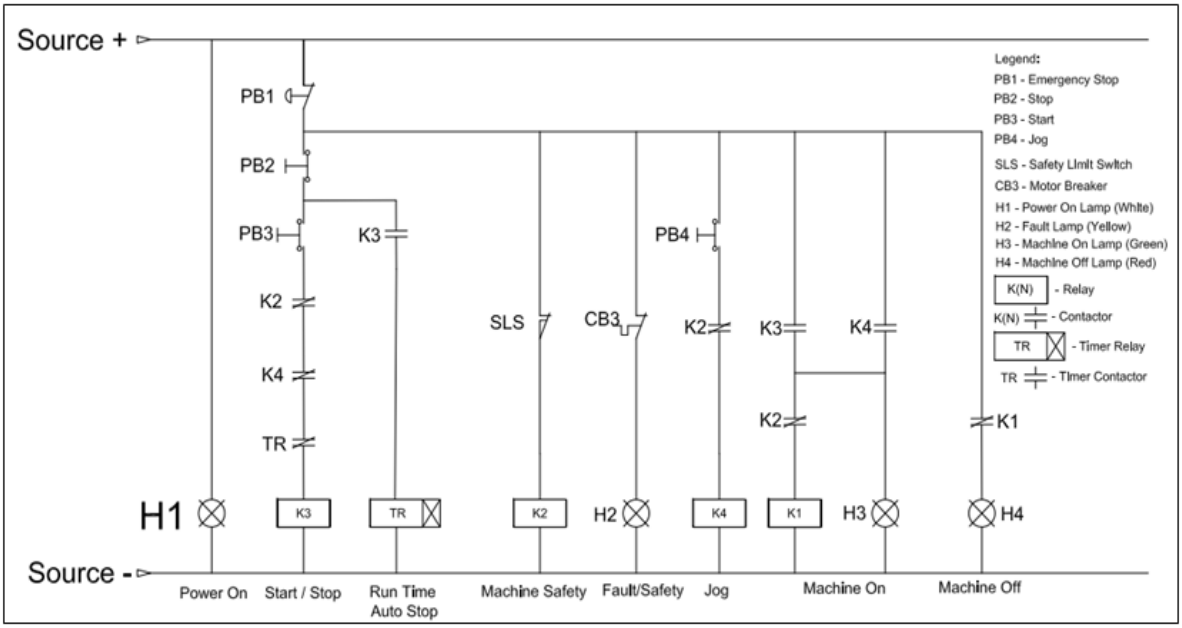

Fig. 4 Control System Schematic Diagram

5. Wires and Overcurrent Protection Devices: To determine the appropriate wire size between the PV module and the SCC, the maximum current I_{max} must first be determined. Section 6.90.2.2.(A)(1) of the PEC states that to calculate I_{max} for the PV system, the I_{SC} of each PV module connected in parallel must be summed and then multiplied by 125 percent [8], resulting in an I_{max} of 1.86 A [24].

$$I_{max} = (\sum Parallel\ PV\ rated\ I_{sc})\ X\ 125\% \quad (8)$$

Equation (8) establishes the basis for sizing the PV module to SCC conductor $I_{PV,\ Conductor}$. In accordance with Section 6.90.2.2. (B)(1), $I_{PV,\ Conductor}$ is equal to 125 percent of I_{max}, resulting in an $I_{PV,\ Conductor}$ of 2.33 A. The wire ampacity used between the PV module and SCC should be greater than 2.33 A. Therefore, a 2.0 mm² THHN Cu wire with a 25 A ampacity was used as the PV conductors [24].

$$I_{PV\ Conductor} = I_{max}\ x\ 125\% \quad (9)$$

Based on Section 6.90.2.3.(A)(2), no overcurrent device is necessary for PV modules or PV source circuits if the total ISC from all sources does not exceed the ampacity of the conductors and complies with the maximum overcurrent protective device size rating specified for the PV module [24]. The nameplate ISC and maximum overcurrent protection rating are 1.49 A and 16 A, respectively. Thus, according to the cited section, no overcurrent protection device is required between the PV module and SCC.

Next, when determining the circuit conductor used for SCC to battery and load, the greater current rating between Formula (10) and Section 7.6.2.4 was applied. The total current I_{total} supplied to the load is the sum of the motor control current $I_{motor\ control}$ and the motor's rated full load current $I_{MotorFLA}$, multiplied by a safety factor of 125% (10). According to this, Formula (10) requires a wire ampacity greater than 22.35 A. On the other hand, Section 7.6.2.4 [24] states that if a charge controller is installed, the ampacity of the conductors in the output circuit must be based on the maximum rated continuous output current of the charge controller for the selected output voltage range. Therefore, the wire ampacity must be greater than the SCC's maximum rated continuous output current of 20 A. Consequently, the wire size used from SCC to battery and load is based on Formula (10). As a result, 2.0 mm² THHN Cu wire with a 25 A ampacity was also used from SCC to battery and load [24].

$$I_{feeders} = I_{motor\ control} + Motor_{FLA}\ x\ 125\% \quad (10)$$

The overcurrent protection device, which serves as the main breaker to isolate the SCC from the loads, was also based on Formula (10) and the resulting wire size. Consequently, a 20 A circuit breaker rating was chosen for the main breaker. The wire size that feeds current to the motor was calculated in accordance with Section 4.30.2.3.(B) [24], where the ampacity of the conductor must be at least 125% of the nameplate current rating for a varying duty motor (11). Therefore, 2.0 mm² THHN Cu wire with a 25 A ampacity was used, as Formula (11) yields 16.75 A.

$$I_{motor} = Motor_{FLA}\ x\ 125\% \quad (11)$$

Meanwhile, an adjustable instantaneous trip circuit breaker with a range of 10 A to 16 A was used for the motor branch-circuit short-circuit and ground-fault protection. According to Section 4.30.4.2.(B) [24], among other short-circuit and ground-fault protection devices, an adjustable instantaneous trip circuit breaker, also known as a motor-circuit protector, is allowed as long as the setting is adjusted to no more than 250% of the full-load current of the motor.

The conductors employed in the motor control circuit, which connect various controller components such as timers, relays, and LED lights, use 0.75 mm² Cu wire. This wire gauge was chosen because the motor control, during its initial testing, drew a current of less than 1 A. As for the overcurrent protection device, Section 4.30.6.2.(B)(1) [24] stipulates that if the motor's overcurrent protective device fails to offer protection to the motor control circuit, a separate safeguard must be implemented. Importantly, this additional overcurrent protection should not exceed 7 A for 0.75 mm² Cu wire. Hence, a 4 A rating of overcurrent protection was used.

D. Data Gathering and Treatment

In gathering the data needed for the objective, the machine was tested by loading it in increments of 4 kg from 0 kg to 20 kg. The following parameters were measured at each load increment of 4 kg: voltage, current, speed, and continuous output torque. Voltage and current were measured using both digital and analog voltage and current meters, speed in rpm was measured using a tachometer, and continuous output torque was measured using a torque sensor coupled with a dynamometer to vary the load.

Three primary indicators based on physical appearance were used to determine if food waste has turned into compost [25]: (1) Color: The compost should have a dark brown color, similar to that of organic fertilizer; (2) Texture: It should be crumbly and moist but not wet; (3) Smell: The compost should have an earthy smell, not a foul or rotting odor. By evaluating these characteristics, one can judge whether the food waste has successfully transformed into compost suitable for use as an organic fertilizer.

Moreover, to determine the efficiency of the motor at each load, the mechanical output was calculated by multiplying the speed ω of the drum (in rad/s) and the continuous output torque T (in Nm) of the motor [13].

$$P_{out} = T\omega = \frac{2\pi NT}{60} \quad (13)$$

To determine the electrical input at each load, the average voltage was multiplied by the average current [14].

$$P_{in} = V_{av}I_{av} \quad (14)$$

Thereafter, the mechanical output of the motor per load increment was divided by the electrical input per load increment and multiplied by 100 percent [15].

$$\eta_{@nth\ load} = \frac{P_{in}}{P_{out}}\ x\ 100\% \quad (15)$$

III. RESULTS AND DISCUSSION

Figures 5 show the variation in voltage and current across the motor under loads of 0 kg, 4 kg, 8 kg, 12 kg, 16 kg, and 20 kg. It is evident from the figures that the voltage has an inverse proportional relationship with the load, as the voltage continuously dropped from 24.8 V to 23.3 V with increasing load from 0 kg to 20 kg.

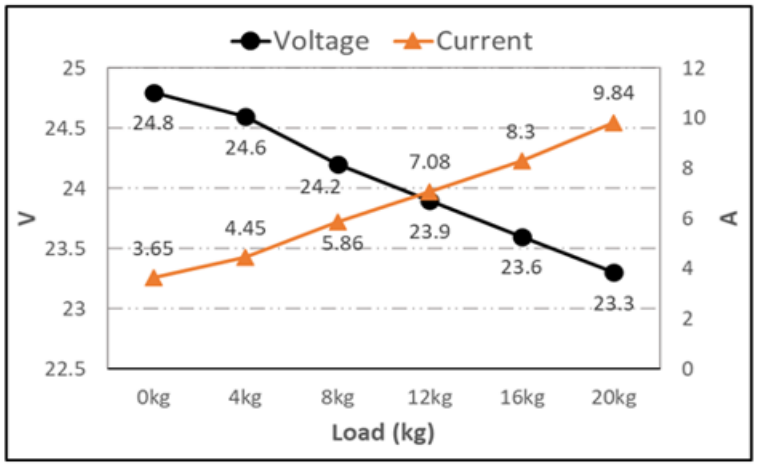

Fig. 5 Voltage and current at different loads

Meanwhile, the current has a direct proportional relationship with the load, increasing from 4.1 A to 9.84 A as the load increased from 0 kg to 20 kg. This increase in current with respect to the load is due to the motor requiring more torque to overcome resistance and maintain speed. To produce more torque, the motor draws more current from the power source to generate a stronger magnetic field. Consequently, the voltage also drops accordingly. As the current increases, the voltage drop across the internal resistance of the battery also increases, affecting the terminal voltage of the battery, which is the applied voltage across the motor terminals [19, 26]. This variation in voltage is acceptable according to the National Electrical Manufacturers Association (NEMA). According to NEMA MG1-2016, Section 12.44.1, motors are electrically designed around the expected supply voltage with a tolerance of +/-10% voltage maximum for small- and medium-voltage electric motors.

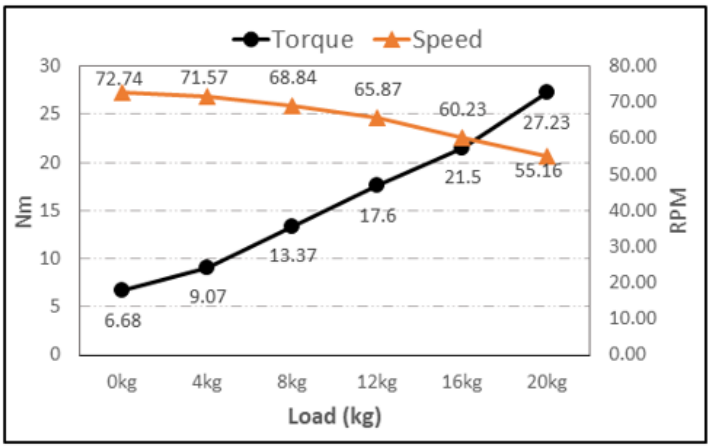

Fig. 6 Torque and Speed at Different Loads

Figure 6 shows the variation in continuous output torque and speed of the motor under loads of 0 kg, 4 kg, 8 kg, 12 kg, 16 kg, and 20 kg. The relationship between torque and speed with the load indicates that the torque and speed of the motor have direct and inverse proportional relationships with the load, respectively. Specifically, the torque of the motor increased from 6.68 Nm to 27.23 Nm as the load increased from 0 kg to 20 kg. This increase in torque arises to overcome the load and maintain rotational motion. Conversely, as the load increases, the motor speed decreases from 72.4 rpm to 55.16 rpm. According to [19, 26], this reduction in speed is due to the decrease in back EMF, which allows more current to flow through the windings to maintain torque. However, this increase in current results in a larger voltage drop across the internal resistance of the motor, further reducing the effective voltage available for driving the motor.

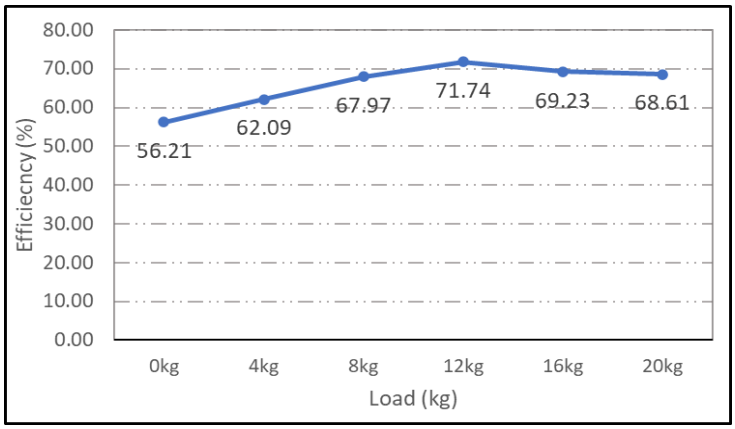

Fig. 7 Efficiency of the Motor

Figure 7 shows the efficiency of the motor relative to the drum load. It can be observed that the efficiency increases with the load until reaching a maximum at 12 kg. Beyond this point, the efficiency begins to decline as the load continues to increase up to 20 kg.

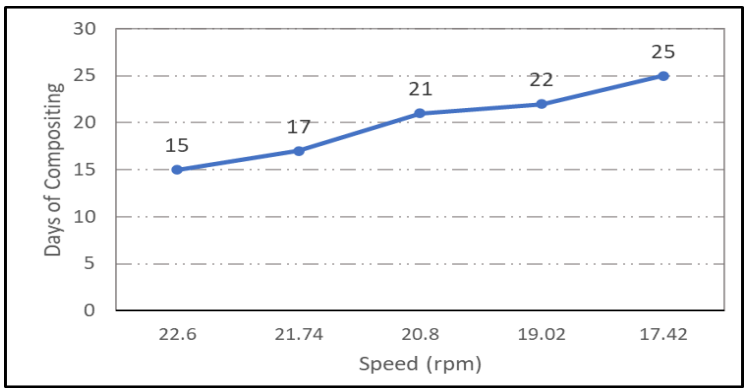

Fig. 8 Days of Composting and Rotational Speed

Figure 8 indicates a negative correlation between the days of composting and the speed of the rotating drum. For instance, at 22.6 RPM, the composting time is at its lowest of 15 days. As the speed decreases to 21.74 RPM, the composting time increases to 17 days. Further reductions in speed to 20.8 RPM, 19.02 RPM, and 17.42 RPM result in composting times of 21 days, 22 days, and 25 days, respectively. These findings indicate that slower speeds yield longer composting times, which aligns with the results of studies [11] and [12]. These studies state that the aeration rate, which depends on drum speed or turning frequency, affects the maturity of the compost.

IV. CONCLUSION AND RECOMMENDATION

In conclusion, the experimental analysis of the motor under varying loads reveals several significant relationships between voltage, current, torque, speed, and efficiency. The voltage exhibits an inverse proportional relationship with load, steadily decreasing as the load increases, while the current shows a direct proportional relationship, consistently rising with increased load. This phenomenon occurs as the motor demands more torque to overcome resistance and maintain its rotational speed, leading to an increase in current draw from the power source. Consequently, the voltage drop across the internal resistance of the battery affects the terminal voltage applied across the motor terminals, in accordance with NEMA standards. The torque and speed exhibit direct and inverse proportional relationships with the load, respectively. As the load increases, the torque rises to overcome it, while the speed decreases due to a reduction in back EMF, allowing more current to flow through the windings to maintain torque. However, this increase in current also results in a larger voltage drop across the motor's internal resistance, further diminishing the effective voltage available for driving the motor, which slows it down. Moreover, efficiency initially increases with the load until reaching a peak efficiency point at 12 kg. Beyond this optimal load, efficiency begins to decline as the load continues to increase up to 20 kg. This trend is expected, as the motor operates most efficiently when its load matches its design parameters, deviations from this optimal point lead to decreased efficiency. Meanwhile, the days of composting increase as the speed of the drum decreases, indicating a direct relationship between the two.

Further studies might explore the capability of this machine by implementing an effective battery management strategy through a voltage regulator to optimize the balance between discharging (motor operation) and charging (solar panel utilization) to maintain constant voltage throughout. Additionally, opportunities to fine-tune measurement instruments to enhance precision should be explored. System integration and control algorithms could be developed to optimize coordination between the motor, energy storage, and solar panel components. This includes predictive control strategies, dynamic load management, and adaptive power management algorithms.

REFERENCES

[1] Food and Agriculture Organization of the United Nations, "Key facts on food loss and waste you should know!" [Online]. Available: http://www.fao.org/save-food/resources/keyfindings/en/. Accessed: Oct. 18, 2023.

[2] FAO, WFP, IFAD, UNICEF W, "The state of food security and nutrition in the world. Building resilience for peace and food security," *Int. J. Phytoremediation*, 2017. [Online]. Available: https://www.fao.org/3/I7695e/I7695e.pdf.

[3] United Nations, "Food loss and waste reduction," [Online]. Available: https://www.un.org/en/observances/end-food-waste-day. Accessed: Oct. 18, 2023.

[4] E. Ebikade *et al.*, "The future is garbage: repurposing of food waste to an integrated biorefinery," *ACS Sustainable Chem. Eng.*, vol. 8, no. 22, pp. 8124-8136, 2020. [Online]. DOI: 10.1021/acssuschemeng.9b07479.

[5] V. Kumar *et al.*, "Emerging challenges for the agro-industrial food waste utilization: A review on food waste biorefinery," *Bioresour. Technol.*, vol. 362, article 127790, Oct. 2020. [Online]. Available: https://doi.org/10.1016/j.biortech.2022.127790.

[6] U.S. Energy Information Administration, "U.S. energy facts explained - consumption and production," [Online]. Available: https://www.eia.gov/energyexplained/us-energy-facts/. Accessed: Oct. 18, 2023.

[7] Department of Health and Department of Social Welfare and Development, "Environmental and Social Management Framework The Philippine Multi-sectoral Nutrition Project," 2022. [Online]. Available: https://kalahi.dswd.gov.ph/phocadownload/Philippine%20Multisectoral%20Nutrition%20Project%20%20Environmental%20and%20Social%20Management%20Framework,%2011Feb2022.pdf. Accessed: Oct. 18, 2023.

[8] Department of Science and Technology - Food and Nutrition Research Institute (DOST-FNRI), "Consumption Survey," 2022. [Online]. Available: http://enutrition.fnri.dost.gov.ph/site/uploads/2018-2019%20Facts%20and%20Figures%20%20Food%20Consumption%20Survey.pdf. Accessed: Oct. 18, 2023.

[9] L. H. Anh *et al.*, "Site-specific determination of methane generation potential and estimation of landfill gas emissions from municipal solid waste landfill: A case study in Nam Binh Duong, Vietnam," *Biomass Convers. Biorefinery*, vol. 12, pp. 1-12, Mar. 15, 2021. [Online]. Available: https://www.researchgate.net/publication/350074312_Site-specific_determination_of_methane_generation_potential_and_estimation_of_landfill_gas_emissions_from_municipal_solid_waste_landfill_a_case_study_in_Nam_Binh_Duong_Vietnam.

[10] Y. Lv *et al.*, "Anaerobic co-digestion of food waste with municipal solid waste leachate: A review and prospective application with more benefits," *Resour., Conserv. Recycl.*, vol. 174, article 105832, 2021. [Online]. Available: https://doi.org/10.1016/j.resconrec.2021.105832.

[11] Y. Wang *et al.*, "Aeration rate improves the compost quality of food waste and promotes the decomposition of toxic materials in leachate by changing the bacterial community," *Bioresour. Technol.*, vol. 340, article 125716, Nov. 2021. [Online]. DOI: 10.1016/j.biortech.2021.125716.

[12] A. S. Kalamdhad and A. A. Kazmi, "Effects of turning frequency on compost stability and some chemical characteristics in a rotary drum composter," *Chemosphere*, vol. 74, no. 10, pp. 1327-1334, 2009. [Online]. Available: https://doi.org/10.1016/j.chemosphere.2008.11.058.

[13] L. Peng *et al.*, "Effect of aeration rate, aeration pattern, and turning frequency on maturity and gaseous emissions during kitchen waste composting," *Environ. Technol. Innov.*, vol. 29, article 102997, 2023. [Online]. Available: https://www.sciencedirect.com/science/article/pii/S2352186422004205.

[14] R. Tang *et al.*, "Effect of moisture content, aeration rate, and C/N on maturity and gaseous emissions during kitchen waste rapid composting," *J. Environ. Manage.*, vol. 326, article 11666, 2023. [Online]. Available: https://www.sciencedirect.com/science/article/abs/pii/S0301479722022356.

[15] T. Sayara *et al.*, "Home composting of food wastes using rotary drum reactor as an alternative treatment option for organic household wastes," *J. Ecol. Eng.*, vol. 23, no. 6, pp. 139-147, 2022. [Online]. DOI: 10.12911/22998993/147873.

[16] F. Z. Siti *et al.*, "Autonomous solar rotary composter equipped with a remote management system," in *2021 9th Int. Renewable Sustainable Energy Conf. (IRSEC)*, IEEE, pp. 1-5, Nov. 2021. DOI: 10.1109/IRSEC53969.2021.9741218.

[17] M. M. Lahmadi *et al.*, "New ecological composter powered by solar panels without battery to produce organic fertilizers," *Int. J. Emerging Technol. Adv. Eng.*, vol. 12, no. 9, pp. 14-22, 2022. DOI: 10.46338/ijetae0922_02.

[18] T. Sayara *et al.*, "Recycling of organic wastes through composting: Process performance and compost application in agriculture," *Agronomy*, vol. 10, article 1838, Nov. 22, 2022. [Online]. Available: https://doi.org/10.3390/agronomy10111838.

[19] C. S. Siskind, *Electrical Machines*, 2nd ed. New York, NY, USA: McGraw-Hill, 1959, p. 59.

[20] P. L. Mangeshkar and T. G. Manohar, "Design and analysis of optimal maximum power point tracking algorithm using ANFIS controller for PV systems," *Asian J. Electr. Sci.*, vol. 8, no. 3, pp. 11-17, 2019. [Online]. Available: https://doi.org/10.51983/ajes-2019.8.3.2103.

[21] S. O. Ejiko and D. Olaniyi, "Development of regression models for appropriate battery banking determination in solar power system," *IOSR J. Electr. Electron. Eng.*, vol. 13, no. 1, ver. III, pp. 30-37. [Online]. Available: https://www.iosrjournals.org/iosr-jeee/Papers/Vol13%20Issue%201/Version-3/E1301033037.pdf.

[22] N. A. Priya *et al.*, "Performance analysis of a high gain LUO converter-based hybrid PV-wind system," *Asian J. Electr. Sci.*, vol. 10, no. 1, pp. 1-4, 2021. [Online]. Available: https://doi.org/10.51983/ajes-2021.10.1.2794.

[23] S. Ahmed, "Unlocking rooftop solar in the Philippines: Energy-supply security and lower electricity costs," *Energy Finance Analyst*, Aug. 2018, pp. 10. [Online]. Available: https://ieefa.org/wp-content/uploads/2018/08/IEEFA_Unlocking-Rooftop-Solar-in-the-Philippines_August-2018.pdf.

[24] *Philippine Electrical Code*, 2017th ed., Institute of Integrated Electrical Engineers.

[25] S. Osmanski and S. Osmanski, "Is your compost finished? Signs your compost is ready to use," *Green Matters*, Nov. 10, 2020. [Online].

[26] V. K. Mehta and R. Mehta, *Principles of Electrical Machines*. India: S Chand & Company Limited, 2002.